Journal of Physical Chemistry A
jp-2010-04246k
Accepted July 12, 2010

Computational Strategies for Reactions of Aggregated and Solvated Organolithium Carbenoids

B. Ramachandran, [a,*] Purnima Kharidehal,[a] Lawrence M. Pratt, [b] Stewart Voit, [b] Fabian N. Okeke,[b] and Monique Ewan[b]

(a) Institute for Micromanufacturing, Louisiana Tech University, Ruston, Louisiana 71272, USA
(b) Department of Chemistry, Fisk University, 1000 17th Ave. N., Nashville, Tennessee 37209, USA

ABSTRACT

This study explores the degree to which GGA, meta-GGA, hybrid GGA, and hybrid meta-GGA functionals of Density Functional Theory, when used with the 6-31+G(d) basis set, are able to reproduce the MP2/6-31+G(d) structures and energetics of the species involved in the reactions of halomethyllithium carbenoids with ethylene. While many popular DFT functionals have been parameterized and/or benchmarked using various databases, the scarcity of experimental structural and energetic information for organolithium compounds have resulted in their exclusion from these training and test sets. In this work, we first establish a set of *practical* benchmark reaction energetics against which the performance of DFT methods for larger molecules can be compared. Next, we examine the performance of 13 DFT functionals spanning the second, third, and fourth rungs of the "Jacob's ladder" using 84 molecules and 78 reactions. The main conclusions are (a) the meta-hybrid GGA M06-2X is the best functional among the set for organolithium chemistry, (b) the hybrid GGA PBE1PBE consistently yields equilibrium and transition state geometries that are very close to the MP2 predictions, and (c) MP2//M06-L or MP2//PBE1PBE model chemistries are excellent low-cost alternatives to the costly MP2. However, this work also showed that the very popular B3LYP functional is a rather poor choice for these systems.

* ramu@latech.edu

1. Introduction

The development of orbital-dependent Density Functional Theory (DFT)[1,2] has reached the point where many functionals achieve comparable accuracy in atomization energies, ionization potentials, electron affinities, thermochemistry, and reaction barriers as methods based on post-Hartree-Fock wave function theory (WFT) at comparable or lesser computational cost.[3] Extensive databases incorporating experimental data and high-level *ab initio* calculations, such as the Gaussian training sets,[4] the Minnesota databases of the Truhlar group,[5] and the Weizmann 1-4 databases[6,7,8,9,10] have been used to parameterize new functionals or to evaluate their performance relative to other methods.

Conspicuously missing from these databases are organolithium compounds. One reason for their exclusion is clearly the scarcity of experimental thermochemical data. A second and equally important reason is that it is nearly impossible to compute high-level *ab initio* (i.e., WFT methods that systematically account for dynamical correlation used with large, polarized basis sets) data for the dominant reactive species in the reactions of organolithum compounds and their transition states, because of the need to consider rather large aggregates of molecules. In this paper, we examine the performance of 13 modern DFT functionals, when used with a double-zeta quality polarized basis set, in predicting the geometries and energetics relevant for the reactions of halomethyllithium carbenoids (Li-CH_2-X; X = F, Cl, Br) with ethylene to produce cyclopropane. In the following paragraphs, we summarize the reasons for our interest in these reactions and our decision to use them as a test bed for evaluating the performance of DFT functionals.

Organolithium carbenoids are among the reagents of choice for inserting a CH_2 group into a C-C double bond in a stereospecific manner, typically yielding almost complete reaction and high

yields under extremely mild (–110 °C to –20 °C) conditions. The precise mechanism for this process —direct insertion (methylene transfer) or a step-wise carbolithiation pathway— was unclear until recently. Experiments appeared to support the concerted pathway[11,12] but the first computational study of the reaction

$$\text{Li-CH}_2\text{-Cl} + \text{H}_2\text{C=CH}_2 \rightarrow \text{Cyclopropane} + \text{LiCl} \qquad (1)$$

by Nakamura et al.[13] indicated that the stepwise pathway actually had a lower reaction barrier. Recently, from the work of Ke, Zhao, and Phillips[14] and our own work,[15] it became clear that aggregation states of the organolithium reagents have a very strong influence on the reaction barrier heights. In Ref. 15, we reported zero point energy inclusive MP2/6-31+G(*d*) reaction barriers $\Delta U_0^{\ddagger}$ of 8.5 kcal/mol and 6.4 kcal/mol, respectively, for the concerted (labeled TS **1** in Ref. 15 and in this paper) and stepwise (TS **2** in Ref. 15 and in this paper) pathways of Eq. (1), in qualitative agreement with the results of Nakamura et al.[13] However, in reality, the dimeric $(\text{Li-CH}_2\text{-Cl})_2$ is considerably more stable. Two dimeric species, labeled **6** and **7** in Ref. 15, were identified, and the $\Delta U_0^{\ddagger}$ for the reaction of **6** (**7**) with ethylene by the direct and stepwise pathways are 10.01 (7.50) and 24.62 (18.72) kcal/mol, respectively, showing a clear preference for the direct pathway. The B3LYP/6-311G(d,p) results of Ref. 14 are qualitatively similar and, indeed, we note that Ref. 14 is the first study to quantitatively establish the influence of aggregation states in determining the reaction pathway in organolithium chemistry. Therefore, consideration of aggregated molecules is essential to understand the reactivity and reaction mechanisms of organolithium compounds. Another challenging aspect of this class of reagents is the strong coordination of lithium with the electronegative atoms in moderately polar solvent molecules such as dimethyl ether or tetrahydrofuran (THF). The steric effects of the strongly

coordinated solvent molecules play an important role in determining the relative stability and reactivity of the aggregates. For example, $(LiCH_2X)_2 \cdot 4THF$ appears to be unable to react with ethylene due to the steric effects of the coordinated solvent molecules, and needs to first dissociate to $(LiCH_2X)_2 \cdot 3THF$ prior to forming transition states for the direct or stepwise pathways.[15] A second example of the steric effect of solvation is that the intrinsic reaction coordinate of the gas phase monomers and dimers pass through rather deep minima corresponding to pre-reactive complexes between ethylene and the carbenoid whereas the THF-solvated species appear to be unable to form such complexes. Also, the tetrameric species $(LiCH_2X)_4$ was found to be much more stable than the dimer in nonpolar solvents but it is less stable than the dimer in THF, due to the increased steric effects of the strongly coordinated solvent.[15] Continuum solvation models obviously cannot account for these effects. Therefore, in addition to the aggregation of the organolithium reagents, the first solvation sphere also needs to be explicitly considered in computational treatments of reactions in ethereal solvents. These requirements significantly increase the size of the systems that need to be studied (each THF molecule adds 13 atoms).

Because of the challenges described above, among the WFT methods that systematically include dynamic correlation energy, only the MP2 with a modest basis set is practical for routine study of organolithium species. However, even MP2 geometry optimizations and frequency calculations for large molecules require considerable computational resources. As noted earlier, modern DFT functionals tend to be less demanding computationally, but their reliability remains to be systematically studied in the context of organolithium species. The forces responsible for aggregation and coordination to ethereal solvents are due to non-bonded interactions driven by electron polarization. Moreover, in all aggregates, the lithium is “hypervalent” in the sense that

it strongly interacts with more than one atom. Such interactions have been found to be challenging for most DFT functionals. In the course of the computations performed for the work reported in Ref. 15, we discovered significant disparities in molecular geometries and relative energies between the predictions of the popular B3LYP[16] functional and MP2 for THF-solvated and aggregated species. This motivated us to conduct a systematic examination of the performance of several popular DFT functionals using the reactions of aggregated halomethyllithium carbenoids in the gas phase (or nonpolar solvents) and THF solvent as a test bed. This paper is a report of that study.

The relative performance of the methods are evaluated using 84 molecules, out of which 33 include coordinated THF solvent molecules, 45 gas phase reactions of $(LiCH_2X)_n$; X = F, Cl, Br, n = 1 or 2, and 33 reactions of $(LiCH_2X)_n \cdot m$THF; m = 0, 2, 3, or 4. The data used for performance evaluation include MP2 single point energies at DFT-optimized geometries ($E_{MP2//DFT}$), the reaction energies ΔE (the difference in the Born-Oppenheimer energies of the products and reactants), and the barrier heights $\Delta E^{\ddagger}$, the difference in energy between the saddle points and the reactants. The test set includes 36 transition states, 24 in the gas phase and 12 in THF solution. The gas phase test set includes 9 pre-reactive complexes which display long-range non-bonded interactions between the Li atom and the ethylene double-bond. The organolithium species in the condensed phase have strong coordination between the Li and the oxygen atoms of THF as well as the interactions with ethylene. Overall, we believe that this test set offers a set of diverse challenges for the DFT functionals tested, many of which may not be represented in the training sets used to parameterize them or to evaluate their relative performances.

The remainder of this paper is organized as follows. In Section 2, we describe the methodology used for establishing the performance yardsticks, the DFT functionals examined, and the molecules and reactions used as the test bed. In Section 3, we present the results and discuss them. We conclude in Section 4 with a summary of the main conclusions drawn from this work.

2. Calculations

2. A. Performance benchmarks

In the absence of reliable experimental data, high-level *ab initio* calculations are the standard procedure for creating benchmarks against which the performance of various methods and basis sets can be evaluated. An excellent example of such a benchmark is the DBH24/08 database of reaction barrier heights of Zheng, Zhao, and Truhlar,[3] based on W4 or W3.2 values.[10] However, the size of the systems typically encountered in organolithium chemistry does not lend itself easily to computations using high-level WFT methods and large basis sets. Instead, we describe how a reasonably accurate set of "benchmark" reaction energetics can be computed using MP2/6-31+G(d) geometries as the basis.

We first establish the quality of the structures obtained at MP2/6-31+G(d) level of theory for 13 small molecules involved in the reactions studied [$LiCH_2F$, $LiCH_2Cl$, $LiCH_2Br$, TS **1** (F, Cl, Br), TS **2** (F, Cl, Br), LiCl, ethylene, cyclopropane, and THF] against the QCISD/6-311G(d,p) geometries. The geometries for the first 9 molecules were optimized starting from MP2/6-31+G(d) geometries and the last four were taken from the Computational Chemistry Comparison and Benchmark Database maintained by NIST.[17] Two measures are employed in this evaluation: (a) comparison of the MP2/6-31+G(d) single point energy of the QCISD/6-311G(d,p) structures with that of the MP2/6-31+G(d) optimized structure, and (b) comparison of the geometric parameters (bond lengths, bond angles, and dihedral angles) of the equilibrium structures

obtained by the two methods. **Table I** summarizes the results of this analysis. The maximum difference between the $E_{\text{MP2/6-31+G(d)}}$ and $E_{\text{MP2/6-31+G(d)//QCISD/6-311G(d,p)}}$ among these four molecules is only 0.4 kcal/mol (for $LiCH_2Br$ TS **1**) and the average difference is 0.17 kcal/mol. Structural comparisons between the QCISD/6-311G(d,p) and MP2/6-31+G(d) equilibrium geometries for these four molecules also confirm that the geometry differences are quite small. Therefore, we conclude that MP2/6-31+G(d) geometries can be used as the standard against which DFT geometries can be evaluated.

Returning to the subject of benchmark energetics, the reaction energies ΔE and the barrier heights $\Delta E^{\ddagger}$ for the 8 reactions of $(LiMeCl)_2$ with ethylene at MP2/6-31+G(d), MP2/6-311+G(2df,2p) and CCSD(T)/6-31+G(d) levels of theory are tabulated in **Table II**, where all the molecular and transition state geometries are optimized at the MP2/6-31+G(d) level. These reactions were selected because they incorporate various types of interactions, such as those responsible for the formation of dimers, pre-reactive complexes, and transition states. The types of structures involved in these reactions and the numbering scheme used to refer to the molecules and transition states are shown in **Figure 1**. Each pre-reactive complex (or pre-complex) numbered **n′** is a true minimum between the reactants and the transition state labeled TS **n**.[18]

The calculations summarized in Table II allow us to establish a benchmark for *relative* energies, i.e., ΔE values, using the relationship

$$\Delta E_{\text{benchmark}} = \Delta E_{\text{MP2/6-311+G(2df,2p)//6-31+G(d)}} + [\Delta E_{\text{CCSD(T)/6-31+G(d)}} - \Delta E_{\text{MP2/6-31+G(d)}}] \qquad (2)$$

which is similar in spirit to the strategy reported by Zhao and Truhlar for generating benchmarks for evaluating various methods.[19,20,21] However, even the benchmark in Eq. (2) is impractical for

the aggregated and THF-solvated species whose reactions we wish to examine, since CCSD(T) calculations even with a modest basis set would be extremely difficult, if not impossible, for the large molecules involved. Therefore, in Table II, we also report the absolute difference $|\Delta E_{\text{benchmark}} - \Delta E_{\text{MP2/6-31+G(d)}}|$ for the 8 reactions. The average absolute difference is 1.98 kcal/mol, most of which can be attributed to reactions 1 and 2 in which cyclopropane is formed. It turns out that the CCSD(T)/6-31+G(d) atomization energy for cyclopropane, 780.4 kcal/mol, is at considerable variance from the zero-point exclusive experimental value of 853.41 kcal/mol.[22] Since MP2/6-31+G(d) does a slightly better job of reproducing the atomization energy (788.08 kcal/mol), the "benchmark" atomization energy of 831.16 kcal/mol calculated using Eq. (2) is actually worse than the MP2/6-311+G(2df,2p) result of 838.35 kcal/mol. Using $\Delta E_{\text{MP2/6-311+G(2df,2p)}}$ as the benchmark for these two reactions, the average absolute average difference for the 8 reactions decreases to 0.81 kcal/mol, well below the "chemical accuracy" goal of ±1 kcal/mol. Therefore, we adopt $\Delta E_{\text{MP2/6-31+G(d)}}$ as a *compromise* yardstick against which the performance of various DFT "model chemistries" (see below) may be evaluated.

2. B. DFT Functionals and Model Chemistries

The "Jacob's ladder" analogy of Perdew[23,24] is very useful for classifying the nature and sophistication of density functionals. The first rung of the ladder is occupied by local spin density functionals which are generally quite useful in solid state physics but typically lead to large errors for small molecules. The second rung consists of the generalized gradient approximation (GGA) functionals. Of these, we examine PW91PW91,[25] mPWPW91,[26] and PBEPBE.[27] For the remainder of this paper, we shall abbreviate the first and last functionals as PW91 and PBE, respectively. The third rung is occupied by the so-called meta-GGA (m-GGA) functionals which incorporate orbital kinetic energy density. We consider TPSSTPSS[28]

(abbreviated hereafter as TPSS) and M06-L[29] in this category. The fourth rung belongs to the hybrid GGA's (h-GGA) which introduce non-local effects by mixing in exact Hartree-Fock exchange, and hybrid meta-GGA's (h-m-GGA) or hyper-GGA's which, in addition to exact exchange, also incorporate the kinetic energy density of meta-GGA's. In the fourth rung, we consider the h-GGA's B3LYP,[16] B3PW91,[30] mPW1LYP, [26,31] mPW1PW91, [26] and PBE1PBE; [32] and the h-m-GGA's BMK,[33] M06,[34] and M06-2X.[34] The hybrid PBE1PBE has been referred to as PBE0 to emphasize the non-empirical determination of the fraction of exact exchange in the functional (i.e., that it is a hybrid with zero empirical parameters),[32] and we will abbreviate it as PBE0 hereafter.

The term "model chemistry" is generally applied to a single step or multi-step calculation with a specified basis set. In the present work, each of the 13 functionals named above were used with the 6-31+G(d) basis set which may well be the largest practical polarized double-zeta basis with diffuse functions that can be used in geometry optimizations and MP2 calculations with the largest molecules studied. As we have already noted, this basis is sufficient to achieve excellent convergence in geometry and reasonable convergence in reaction energetics at the MP2 level of theory. In addition to the DFT/6-31+G(d) model chemistries, we also consider MP2 single point energy calculations at the DFT/6-31+G(d) optimized geometries, leading to the two-step model chemistry MP2/6-31+G(d)//DFT/6-31+G(d). For the remainder of this paper, the basis set used in the calculations is understood to be 6-31+G(d) unless otherwise specified.

2. C. Methodology

Our test set includes 84 molecules, out of which 33 are coordinated to THF solvent molecules. Using these molecules as reactants, intermediates, transition states, or products, we consider 45 gas-phase reactions and 33 reactions of THF-solvated molecules. The computational

methodology involved two steps: (a) DFT/6-31+G(d) geometry optimization starting from the MP2/6-31+G(d) structure to give DFT/6-31+G(d) energies (where "DFT" will be replaced with the functional used), and (b) MP2/6-31+G(d) single point energy calculation at the equilibrium or saddle point geometry identified in step (a) to give MP2/6-31+G(d)//DFT/6-31+G(d) energies (MP2//DFT hereafter where "DFT" will be replaced with the functional used). All calculations were done with the Gaussian 03[35] and Gaussian 09[36] programs. Structural representations of the different types of gas phase molecules in our test set are shown in Fig. 1. In both gas phase and THF, each type of molecule is present with X = F, Cl, and Br. In THF, each lithium atom is coordinated to two THF molecules except in transition states **8-11**, which are tri-solvated. Three molecules (ethylene, THF, and the lithium halides LiX) are not shown.

We compute the DFT and MP2//DFT reaction energies, dimerization energies, formation of pre-reactive complexes, and barrier heights for the direct (concerted) and stepwise reactions of $(LiCH_2X)_n \cdot mTHF$; X = F, Cl, Br; n = 1 or 2; m = 0, 2, 3, or 4. These are compared with the MP2/6-31+G(d) energies which, as noted in Section 2.A, we have adopted as a compromise benchmark to assess the performance of the model chemistries we have employed. All calculated energies are provided in the Supporting Information.

The MP2//DFT energies serve two purposes in our work: firstly, the agreement between the MP2//DFT and MP2 energies is one measure of the agreement between the optimized geometries predicted by the DFT method and MP2; secondly, the MP2//DFT approach, which involves only a single MP2 energy calculation, is practical even for aggregated and solvated systems of up to ~70-90 atoms and so, we wish to assess the performance of these model chemistries as tools for the routine study of organolithium chemistry.

We first evaluate each DFT functional for its ability to yield stationary point geometries (minima or saddle points) close to those predicted by MP2/6-31+G(d), as measured by $|E_{MP2//DFT} - E_{MP2}|$. The geometry convergence tests described in Section 2.A. give us sufficient justification to assign such a "benchmark" status to MP2 geometries. The second performance measure of each model chemistry is the comparison of the ΔE for a chemical transformation (reaction, dimerization, formation of a pre-reactive complex or transition state) to the corresponding ΔE_{MP2}. Detailed data for individual reactions are provided in the Supporting Information. The tables and figures presented in Section 3 summarize the statistics of our evaluations.

3. Results and Discussion

3. A. Molecular Geometries

We assess the ability of each DFT functional to yield geometries close to those predicted by MP2 by examining $\delta E_{DFT} = |E_{MP2//DFT} - E_{MP2}|$. As noted earlier, the starting point for each geometry optimization is the converged MP2/6-31+G(d) geometry for the species under consideration.

In **Figure 2(a)**, we show the average δE_{DFT}, or $\langle \delta E_{DFT} \rangle$ for 51 gas phase molecules (i.e., none coordinated to THF, but including THF), including 24 transition state structures, for the 13 functionals studied. The functionals are arranged in the figure such that one ascends the rungs of the Jacob's ladder as one moves from left to right. The local functionals PW91, mPWPW91, PBE, and TPSS show the largest deviations (between 0.99 and 0.86 kcal/mol) while the hybrid GGA's PBE0 (0.33 kcal/mol), B3PW91 (0.39 kcal/mol) and mPW1PW91 (0.44 kcal/mol) have the smallest deviations. Among the second and third rung functionals, the meta-GGA M06-L is clearly superior to the others in finding geometries close to those predicted by MP2, yielding an average δE_{DFT} of only 0.69 kcal/mol.

The largest δE_{DFT} for almost all functionals was for the X = Br pre-reactive complex **10′** (Fig. 1) formed from dimer **6**. Excluding PBE and PBE0, the average error for the remaining 11 functionals for this particular molecule is a rather large 7.67 ± 0.29 kcal/mol where the small standard deviation reveals that the individual errors are all quite close in magnitude. The largest error is for B3LYP, δE_{B3LYP} = 8.29 kcal/mol. In sharp contrast, for this molecule, δE_{PBE} = 0.56 kcal/mol and δE_{PBE0} = 0.29 kcal/mol. The largest δE_{PBE} among gas phase molecules is 3.89 kcal/mol for TS **10** (X = Cl), for which PBE0 records the smallest error among all functionals, with δE_{PBE0} = 0.50 kcal/mol. The largest δE_{PBE0} is 3.06 kcal/mol for TS **10** (X = F), for which B3LYP yields the lowest error with δE_{B3LYP} = 0.23 kcal/mol.

THF-solvated species pose more challenges for DFT, because of the many conformations possible with minor differences in the relative orientations of the THF ligands. This is reflected in **Figure 2(b)** where we present the $\langle \delta E_{DFT} \rangle$ for 33 molecules coordinated to THF, including 12 transition state structures, for the 13 functionals studied. The smallest δE_{DFT} in Fig. 1(b) is 1.79 kcal/mol for PBE0, while the GGA mPWPW91 and B3LYP have the highest values at about 3.6 kcal/mol, followed by TPSS at 3.2 kcal/mol. We encountered serious difficulties with the BMK functional in locating the THF-solvated transition state structures of dimeric halomethyllithiums, **8-11**. After many failed attempts, we obtained converged structures with a single imaginary frequency for the case X = F for TS **8** and **10** but not for Cl or Br. Also, TS **9** and **11** proved to be elusive for all three halogens. Rather than exclude this functional completely from consideration at this point, we have simply excluded the solvated transition state energies from the averages in this case. Therefore, the δE_{DFT} of 2.52 kcal/mol for BMK includes only the absolute differences for equilibrium structures.

The largest error among the THF-solvated species was recorded with B3LYP, for the tetrasolvated dimer **6** $(LiCH_2Cl)_2 \cdot 4THF$, which gave δE_{B3LYP} = 11.16 kcal/mol. The smallest error among the 13 functionals for this particular molecule is for PBE0, with δE_{PBE0} = 2.16 kcal/mol. The largest *average* error for a single species among THF-solvated molecules was for the tetrasolvated dimer **7** (4.82 ± 1.40 kcal/mol). For this molecule, the largest single error is with B3LYP (7.72 kcal/mol) and the smallest is with PBE0 (2.64 kcal/mol).

The poorer performance of the modified Perdew-Wang (mPW) exchange functional ($\langle \delta E_{mPWPW91} \rangle$ = 3.60 kcal/mol) compared to the original PW91($\langle \delta E_{PW91} \rangle$ = 2.44 kcal/mol) is noteworthy in the context of solvated molecules. Adamo and Barone modified the original Perdew-Wang functional to improve its performance in a variety of situations where attractive noncovalent interactions are involved, such as hydrogen bonds, van der Waals complexes, and charge transfer complexes.[26] It would have been reasonable to assume that such a functional would be dramatically better than PW91 for describing the interactions between the Li atoms and the coordinated THF molecules. We see from Fig. 2(b) that this expectation is not met. The addition of exact Hartree-Fock exchange in the h-GGA mPW1PW91 does lead to a lower $\langle \delta E_{DFT} \rangle$ ($\langle \delta E_{mPW1PW91} \rangle$ = 2.24 kcal/mol) but the performance of this fourth rung h-GGA is not significantly better than the second rung GGA PW91, and is actually worse than the third rung m-GGA, M06-L and the fourth rung PBE0, M06, and M06-2X.

The $\langle \delta E_{DFT} \rangle$ for the 84 molecules, gas phase as well as THF-solvated, calculated using the 13 functionals are presented in **Figure 3**. In Fig. 3, we also show the standard deviation of the differences which provide a measure of the range of distribution of the δE_{DFT} about the average value. PBE0 has the lowest overall average error, with $\langle \delta E_{PBE0} \rangle$ = 0.96± 1.07 kcal/mol, while the

second rung GGA mPWPW91 and fourth rung h-GGA B3LYP have the highest errors of about 2 kcal/mol.

A quantitative summary of the average errors and standard deviations for the gas phase, THF-solvated, and the whole test set of 84 molecules is presented in **Table III**.

3. B. Reaction Energies and Barrier Heights

The performance of the DFT functionals in reproducing *relative energies* in the gas phase is analyzed using reaction energies ΔE, and barrier heights $\Delta E^{\ddagger}$. We define quantities $\delta\Delta E_{\mathrm{DFT}} = |\Delta E_{\mathrm{DFT}} - \Delta E_{\mathrm{MP2}}|$, and $\delta\Delta E_{\mathrm{MP2//DFT}} = |\Delta E_{\mathrm{MP2//DFT}} - \Delta E_{\mathrm{MP2}}|$ for this purpose. As noted in the Introduction, obtaining an MP2 single point energy with a modest basis set at a DFT geometry is a viable option for many large molecules and so we are interested in the performance of such two-step model chemistries.

We have examined 45 gas phase reactions, 24 of which involve the formation of transition states and 9 involve the formation of pre-reactive complexes between the lithium atom and the ethylene double bond. The average $\delta\Delta E_{\mathrm{DFT}}$, or $\langle\delta\Delta E_{\mathrm{DFT}}\rangle$, for the gas phase reactions are presented in **Figure 4(a)** for all 13 functionals. The three clustered bars for each functional represents the overall average (blue), average over reaction energies (red), and average over barrier heights (green). This breakdown allows us to see that although M06-2X gives the lowest error overall, M06-L and PBE0 outperform it if only the reaction energies (red) are considered, and B3LYP does extremely well for barrier heights (green) while doing extremely poorly for reaction energies (red). The h-m-GGA of Boese and Martin, BMK, the only functional in the set which was optimized for kinetics, performs fairly well for barrier heights but rather poorly for reaction energies.

The analysis of two-step model chemistry for gas phase reactions, based on $\langle \delta\Delta E_{\mathrm{MP2//DFT}} \rangle$, is presented in **Figure 4(b)**. The performance in this category is directly related to the consistency with which the functionals predict geometries close to those found by MP2. The superior performance of MP2//PBE0 model chemistry in every category (overall, reaction energies, and barrier heights) in this regard is immediately obvious.

Next we turn to reactions of THF-solvated species. **Figure 5(a)** presents the average $\delta\Delta E_{\mathrm{DFT}}$ for the 33 reactions of THF-solvated species. As noted earlier, in spite of repeated attempts and different approaches, we were unable to converge transition state structures that gave a single imaginary frequency for solvated halomethyllithiums TS **8-11** with the BMK functional. In determining the percentage of exact exchange in the BMK functional, Boese and Martin relied on single point energies calculated at transition state geometries obtained using high-level correlated WFT methods.[33] Therefore, it is possible that the ability of the functional to converge to saddle point geometries, especially in challenging cases, may not have been evaluated. Given these difficulties, we exclude the BMK functional from consideration for these reactions.

The best overall performance for predicting reaction energetics, as judged by the heights of the bars in Fig. 4(a), is given by the m-h-GGA M06-2X, followed by the m-GGA M06-L, and the m-h-GGA M06.

The analysis of two-step model chemistry for the THF-phase reactions, based on $\langle \delta\Delta E_{\mathrm{MP2//DFT}} \rangle$, is presented in **Figure 5(b)**. Once again, M06-2X yields the smallest error, but in this case, the second best performer is the second rung GGA, PW91 followed by M06-L, and PBE0.

The $\delta\Delta E_{DFT}$ for all 78 reactions considered are presented in **Figure 6(a)**. The M06 family of m-h-GGAs take the top three spots. **Figure 6(b)** presents the analysis of the two-step model PBE0 proves to be almost as good as M06-2X, with M06-L taking the third spot. The most widely used h-GGA in existence, the fourth rung B3LYP,[37] performs as poorly as the second rung pure GGA's in Fig. 6(a), and yields the highest $\delta\Delta E_{MP2//DFT}$ in Fig. 6(b).

Table IV summarizes the $\langle\delta\Delta E_{DFT}\rangle$ and $\langle\delta\Delta E_{MP2//DFT}\rangle$ along with the standard deviations for the 45 gas phase, the 33 THF-solvated, and the complete set of 78 reactions examined. For reasons explained above, the reaction barrier statistics for the BMK functional have been omitted in the case of THF-solvated species.

Finally, we examine the performance of the DFT functionals as a function of basis set size using the 8 gas phase reactions tabulated in Table II as a compromise test set (but with $E_{MP2/6\text{-}311+G(2df,2p)}$ energies for reactions 1 and 2, as explained in Section 2A). The mean absolute deviations $\delta\Delta E_{DFT}$ with 6-31+G(d) and 6-311+G(2df,2p) basis sets are shown in **Figure 7**. The third and fourth rung functionals do better than the second rung, as expected. Among the former group, the $\delta\Delta E_{DFT}$ decrease with basis size except for B3LYP, mPW1LYP, and BMK, suggesting that systematic lowering of errors may be possible by using larger basis sets with most of the functionals studied. However, conclusions about the relative performance of the functionals should not be drawn from Fig. 7. The inclusion of THF-solvated molecules in the dataset has a profound influence on the relative errors, and so Fig. 6 is a more reliable guide for the performance of the 13 functionals for *practical* computations on reactions of organolithium compounds.

4. Summary and Discussion

We have examined the performance of 13 DFT functionals spanning the rungs two to four of Perdew's "Jacobs ladder" in an attempt to identify the most accurate and yet economical approach for computational studies of aggregated and solvated organolithium molecules. We use the reactions of $(LiCH_2X)_n \cdot m$THF; X = F, Cl, Br; n = 1 or 2; m = 0, 2, 3, or 4, with ethylene to give cyclopropane as the test bed, using the MP2/6-31+G(d) structures and energies as a *practical* benchmark, which has been validated against higher level methods, for the large molecules involved in our test set.

Our main findings, in the light of the practical benchmark adopted here, are:

a) The h-m-GGA M06-2X is the best functional tested here for a DFT-based study of organolithium reactions, followed closely by M06 and M06-L.

b) The most widely used h-GGA, B3LYP,[37] performs rather poorly for the molecules and reactions investigated. In fact, the overall performance of B3LYP for reaction energetics (Table IV) is comparable to the second rung GGA's.

c) The two step model chemistries MP2//M06-2X and MP2//PBE0 (bottom half of Table IV) yield superior accuracy for reaction energetics, and are attractive alternatives to considerably more resource-intensive MP2 searches for equilibrium geometries and transition states. As revealed in Table III, this is largely a consequence of the superior ability of these functionals to predict geometries very close to those resulting from MP2 optimizations.

d) For reaction energetics, the two step model chemistry MP2//B3LYP (bottom half of Table IV) is the worst performer, yielding average errors larger than two step methods based on second rung GGA's and third rung m-GGA's.

The superior performance of PBE0 is noteworthy from the perspective of functional development through constraint satisfaction. In introducing the PBE functional, Perdew et al. noted:[27] "In contrast to the … PW91 functional, which was designed to satisfy as many exact constraints as possible, the GGA presented here satisfies only those which are energetically significant." The rationale for the 25% exact exchange content in the h-GGA PBE0 was justified *nonempirically* on the basis of the lowest order of the Görling-Levy perturbation theory which provides a realistic description of the adiabatic connection coupling constant dependence of the exchange energy.[32] This approach results in the lowest $\langle \delta E_{\mathrm{DFT}} \rangle$ (Fig. 3) over the set of 84 molecules, and the lowest $\langle \delta \Delta E_{\mathrm{DFT}} \rangle$ [Fig. 6(a)], with the exception of the empirically parameterized M06 family of functionals. The similarity in performance between the PBE and TPSS functionals in Figs 1(a) and comparable performance in Fig. 2(b) can perhaps be attributed to the observation of Tao et al.[28] that "Our functionals are nested ... PBE GGA is inside the TPSS meta-GGA." However, judging by the $\langle \delta E_{\mathrm{DFT}} \rangle$ (Fig. 3) it is disappointing that the inclusion of the positive kinetic energy density in TPSS does not appear to have improved its predictions of equilibrium geometries over PBE for our test set.

Cancellation of errors between the exchange and correlation parts of the functional is often cited as a factor in the satisfactory performance of DFT functionals.[38] The correlation energy for Becke's original parameterization of the B3 exchange functional came from PW91.[30] To create the B3LYP functional, Stephens et al.[16] replaced the PW91 correlation functional with LYP.[31]

Since the LYP functional "does not have an easily separable local component,"[16] the functional III of Vosko, Wilk, and Nusair (VWN)[39] was used in the place of the LSDA local correlation used by Perdew and Wang. The three parameters in the functional were *not* reoptimized after these changes. In spite of the popularity of B3LYP,[37] it is reasonable to expect that these replacements would have affected the cancellation of errors at least in some cases. The better performance of B3PW91 over B3LYP in the present context may be a reflection of this aspect.

It is interesting to consider the progress in the development of density functionals as reflected by the performance measures and the test set used in our work. **Figure 8** shows the average of the errors $\langle \delta\Delta E_{\mathrm{DFT}} \rangle$ and $\langle \delta\Delta E_{\mathrm{MP2//DFT}} \rangle$ for each rung of the Jacob's ladder, and also the $\langle \delta\Delta E_{\mathrm{DFT}} \rangle$ and $\langle \delta\Delta E_{\mathrm{MP2//DFT}} \rangle$ for the best functionals in each rung. These curves confirm the well-documented[1,3,34] improvement in relative energies in going from the local GGA's (second rung) to the non-local h-GGA's and m-h-GGA's. The "best" representatives of each rung outperform the average by appreciable margins. The curves representing the two-step model chemistries show that the performance depends only weakly on the sophistication of the DFT functional used for geometry optimization. However, the steady downward trend of these lines is an indication that the increasing sophistication of the functionals have indeed translated into increased accuracy in geometry prediction.

Despite the justifications provided in Section 2.A, our choice of MP2/6-31+G(d) energies and energy differences as the compromise benchmark, is open to criticism. It can be argued, and indeed evidence exists in other contexts,[40] that many of the higher rung DFT functionals are more accurate than MP2. However, it is unlikely that the *relative* performance of DFT functionals observed in this work would significantly change by a different choice of the

benchmark. If, for example, we were to use M06-2X/6-31+G(d) as the standard against which other model chemistries are compared, the top two curves in Fig. 8 will be displaced downwards by 2.47 kcal/mol so that $\langle \delta \Delta E_{\text{M06-2X}} \rangle = 0$ kcal/mol. However, we have verified that the qualitative features revealed in Fig. 8 will not change except that the two curves representing $\langle \delta \Delta E_{\text{MP2//DFT}} \rangle$ will now be displaced to higher values, reflecting the difference between the MP2//DFT and M06-2X $\langle |\Delta E| \rangle$ values.

Acknowledgements

Grants of CPU time on the IBM p5-575 supercomputers and the Dell PowerEdge Linux clusters of the Louisiana Optical Network Initiative (LONI; http://www.loni.org) are gratefully acknowledged. BR and LMP acknowledge grants of supercomputer time at the National Energy Research Center (NERSC) operated by the Department of Energy (http://www.nersc.gov). LMP acknowledges support for this work by the National Science Foundation through the grant CHE-0643629.

Supporting Information Available: The energies of all reactants, products, pre-reactive complexes, and TS structures from MP2 and all DFT functionals used are provided in an Excel file. This file also contains the list of reactions considered and the reaction energetics calculated from each method. Also included in the file are the calculations of average errors and standard deviations given in Tables III and IV.

References

[1] Sousa, S. F.; Fernandes, P. A.; Ramos, M. J. *J. Phys. Chem. A* **2007**, *111*, 10439.

[2] Kümmel, S; Kronik, L. *Rev. Mod. Phys*. **2008**, *80*, 3.

[3] Zheng, J.; Zhao, Y.; Truhlar, D. G. *J. Chem. Theory Comput*. **2009**, *5*, 808.

[4] Curtiss, L. A.; Raghavachari, K.; Redfern, P. C.; Pople, J. A. *J.Chem. Phys.* **1997**, *106*, 1063; Curtiss, L. A.; Redfern, P. C.; Raghavachari, K.; Pople, J. A. *J.Chem. Phys.* **1998**, 109, 42; Curtiss, L. A.; Raghavachari, K.; Redfern, P. C.; Pople, J. A. *J.Chem. Phys.* **2000**, *112*, 7374; Curtiss, L. A.; Redfern, P. C.; Raghavachari, K.; Pople, J. A. *J. Chem. Phys*. **2001**, *114*, 108.

[5] (a) Lynch, B. J.; Truhlar, D. G. *J. Phys. Chem. A* **2003**, *107*, 3898; (b) *J. Phys. Chem. A* **2003**, *107*, 8996; erratum: **2004**, *108*, 1460.

[6] Martin, J. M. L.; de Oliviera, G. *J. Chem. Phys*. **1999**, *111*, 1843.

[7] Martin, J. M. L. in *Quantum Mechanical Prediction of Thermochemical Data*, Cioslowski, J. Ed., Kluwer, Dordrecht, 2001, p. 31.

[8] Prathiban, S.; Martin, J. M. L. *J. Chem. Phys*. **2001**, *114*, 6014.

[9] Boese, A. D.; Oren, M.; Atasoylu, O.; Martin, J. M. L.; Kállay, M.; Gauss, J. *J. Chem. Phys*. **2004**, *120*, 4129.

[10] Kraton, A.; Rabinovich, E.; Martin, J. M. L.; Ruscic, B. *J. Chem. Phys.* **2006**, *125*, 144108.

[11] U. Burger, R. Huisgen, *Tetrahedron Lett*. **1970**, 3049.

[12] H. C. Stiasny, R. W. Hoffmann, *Chem. Eur. J*. **1995**, *1*, 619.

[13] M. Nakamura, A. Hirai, E. Nakamura, *J. Am. Chem. Soc*. **2003**, *125*, 2341.

[14] Z. Ke, C. Zhao, D. L. Phillips, *J. Org. Chem*. **2007**, *72*, 848.

[15] L. M. Pratt, P. T. T. Tran, N. V. Nguyen, B. Ramachandran, *Bull. Chem. Soc. Japan*, **2009**, *82*, 1107.

[16] Stephens, P. J.; Devlin, F. J.; Chabalowski, C. F.; Frisch, M. J.; *J. Phys. Chem*. **1994**, *98*, 11623.

[17] Johnson III, R. D.; Ed. *NIST Computational Chemistry Comparison and Benchmark Database*, NIST Standard Reference Database Number 101, Release 15, February 2010, http://cccbdb.nist.gov/, last accessed March 11, 2010.

[18] See Figs. 1,2, and Figs. 5-7 of Ref. 15.

[19] Zhao, Y.; Tishchenko, O.; Truhlar, D. G. *J. Phys. Chem. B* **2005**, *109*, 19046.

[20] Zhao, Y.; Truhlar, D. G. *J. Phys. Chem. A* **2006**, *109*, 10478.

[21] Zhao, Y.; Ng, H. T.; Hanson, E. *J. Chem. Theory Comput*. **2009**, *5*, 2726.

[22] Supporting Information for Ref. 5(a).

[23] Perdew, J. P.; Schmidt, K. in *Density Functional Theory and its Application to Materials*, Van Doren, V.; Van Alsenoy, C.; Geerlings, P., Ed. AIP Press, Melville, NY, 2002.

[24] Perdew, J. P.; Ruzsinszky, A.; Constantin, L. A.; Sun, J.; Csonka, G. I. *J. Chem. Theory Comput*. **2009**, *5*, 902.

[25] Perdew, J. P. in *Proceedings of the 21st Annual Symposium on the Electronic Structure of Solids, '91*; Ziesche, P.; Eschig, H., Eds. Akademie Verlag: Berlin, 1991, p. 11; Perdew, J. P.; Wang, Y. *Phys. Rev. B*, **1992**, *45*, 13244.

[26] Adamo, C.; Barone, V.; *J. Chem. Phys*. **1998**, *108*, 664.

[27] Perdew, J. P.; Burke, K.; Ernzerhof, M. *Phys. Rev. Lett.* **1996**, *77*, 3865; *ibid*., **1997**, *78*, 1396 (E).

[28] Tao, J.; Perdew, J. P.; Staroverov, V. N.; Scuseria, G. E. *Phys. Rev. Lett*. **2003**, *91*, 146401.

[29] Zhao, Y.; Truhlar, D. G. *J. Chem. Phys*. **2006**, *125*, 194101.

[30] Becke, A. D.; *J. Chem. Phys* **1993**, *98*, 5648.

[31] Lee, C.; Yang, W.; Parr, R. G. *Phys. Rev. B* **1988**, *37*, 785.

[32] Perdew J. P.; Ernzerhof, M.; Burke, K. *J. Chem. Phys*. **1996**, *105*, 9982.

[33] Boese, A. D.; Martin, J. M. L. *J. Chem. Phys*. **2004**, *121*, 3405.

[34] Zhao, Y.; Truhlar, D. G. *Theor. Chem. Accts*. **2008**, *120*, 215; *Acct. Chem. Res*. **2008**, *41*, 157.

[35] Gaussian 03, Revision C.02, Frisch, M. J.; Trucks, G. W.; Schlegel, H. B.; Scuseria, G. E.; Robb, M. A.; Cheeseman, J. R.; Montgomery, Jr., J. A.; Vreven, T.; Kudin, K. N.; Burant, J. C.; Millam, J. M.; Iyengar, S. S.; Tomasi, J.; Barone, V.; Mennucci, B.; Cossi, M.; Scalmani, G.; Rega, N.; Petersson, G. A.; Nakatsuji, H.; Hada, M.; Ehara, M.; Toyota, K.; Fukuda, R.; Hasegawa, J.; Ishida, M.; Nakajima, T.; Honda, Y.; Kitao, O.; Nakai, H.; Klene, M.; Li, X.; Knox, J. E.; Hratchian, H. P.; Cross, J. B.; Bakken, V.; Adamo, C.; Jaramillo, J.; Gomperts, R.; Stratmann, R. E.; Yazyev, O.; Austin, A. J.; Cammi, R.; Pomelli, C.; Ochterski, J. W.; Ayala, P. Y.; Morokuma, K.; Voth, G. A.; Salvador, P.; Dannenberg, J. J.; Zakrzewski, V. G.; Dapprich, S.; Daniels, A. D.; Strain, M. C.; Farkas, O.; Malick, D. K.; Rabuck, A. D.; Raghavachari, K.; Foresman, J. B.; Ortiz, J. V.; Cui, Q.; Baboul, A. G.; Clifford, S.; Cioslowski, J.; Stefanov, B. B.; Liu, G.; Liashenko, A.; Piskorz, P.; Komaromi, I.; Martin, R. L.; Fox, D. J.; Keith, T.; Al-Laham, M. A.; Peng, C. Y.; Nanayakkara, A.; Challacombe, M.; Gill, P. M. W.; Johnson, B.; Chen, W.; Wong, M. W.; Gonzalez, C.; and Pople, J. A.; Gaussian, Inc., Wallingford CT, 2004.

[36] Gaussian 09, Revision A.1, Frisch, M. J.; Trucks, G. W.; Schlegel, H. B.; Scuseria, G. E.; Robb, M. A.; Cheeseman, J. R.; Scalmani, G.; Barone, V.; Mennucci, B.; Petersson, G. A.; Nakatsuji, H.; Caricato, M.; Li, X.; Hratchian, H. P.; Izmaylov, A. F.; Bloino, J.; Zheng, G.; Sonnenberg, J. L.; Hada, M.; Ehara, M.; Toyota, K.; Fukuda, R.; Hasegawa, J.; Ishida, M.; Nakajima, T.; Honda, Y.; Kitao, O.; Nakai, H.; Vreven, T.; Montgomery, Jr., J. A.; Peralta, J. E.; Ogliaro, F.; Bearpark, M.; Heyd, J. J.; Brothers, E.; Kudin, K. N.; Staroverov, V. N.; Kobayashi, R.; Normand, J.; Raghavachari, K.; Rendell, A.; Burant, J. C.; Iyengar, S. S.; Tomasi, J.; Cossi, M.; Rega, N.; Millam, N. J.; Klene, M.; Knox, J. E.; Cross, J. B.; Bakken, V.; Adamo, C.; Jaramillo, J.; Gomperts, R.; Stratmann, R. E.; Yazyev, O.; Austin, A. J.; Cammi, R.; Pomelli, C.; Ochterski, J. W.; Martin, R. L.; Morokuma, K.; Zakrzewski, V. G.;

Voth, G. A.; Salvador, P.; Dannenberg, J. J.; Dapprich, S.; Daniels, A. D.; Farkas, Ö.; Foresman, J. B.; Ortiz, J. V.; Cioslowski, J.; Fox, D. J. Gaussian, Inc., Wallingford CT, 2009.

[37] See Figure 1 of Ref. 1.

[38] *Introduction to Computational Chemistry*, F. Jensen, Wiley, Chichester, UK 1999, p. 180.

[39] Vosko, S. H.; Wilk, L.; Nusair, M. *Can. J. Phys*. **1980**, *58*, 1200.

[40] For example, see the tables in Ref. 3.

Table I. Comparison of the geometric parameters of optimized structures obtained by QCISD/6-311G(d,p) and MP2/6-31+G(d).

	$\lvert\Delta E\rvert$[(a)] (kcal/mol)	$\langle\lvert\Delta r\rvert\rangle$[(b)] Å	$\max\{\lvert\Delta r\rvert\}$ Å	$\langle\lvert\Delta\theta\rvert\rangle$[(b)] deg	$\max\{\lvert\Delta\theta\rvert\}$ deg	$\langle\lvert\Delta\phi\rvert\rangle$[(b)] deg	$\max\{\lvert\Delta\phi\rvert\}$ deg
LiCl	0.167	0.0403	0.0403	-	-	-	-
Ethylene	0.006	0.0017	0.0017	0.0080	0.0119	(c)	(c)
Cyclopropane	0.029	0.002	0.005	0.010	0.020	0.006	0.012
THF	0.195	0.004	0.014	0.411	0.775	0.427	1.256
$LiCH_2F$	0.287	0.019	0.041	0.699	1.532	0.373	0.742
$LiCH_2Cl$	0.019	0.027	0.063	1.186	1.483	3.143	3.623
$LiCH_2Br$	0.046	0.023	0.052	0.972	1.331	2.386	2.866
TS **1**: $LiCH_2F$	0.101	0.011	0.045	0.883	3.822	0.561	2.760
TS **1**: $LiCH_2Cl$	0.267	0.012	0.046	0.826	4.636	1.330	3.055
TS **1**: $LiCH_2Br$	0.395	0.012	0.041	1.018	5.532	0.788	3.199
TS **2**: $LiCH_2F$	0.222	0.009	0.027	0.554	1.140	0.729	2.294
TS **2**: $LiCH_2Cl$	0.221	0.008	0.038	0.765	2.217	2.781	7.266
TS **2**: $LiCH_2Br$	0.218	0.009	0.038	1.155	3.920	4.152	10.380
Average	0.167	0.0138	0.0347	0.7074	2.2017	1.5159	3.4049

a) The absolute difference between the MP2/6-31+G(d) energies calculated at the QCISD/6-311G(d,p) optimized geometry and the MP2/6-31+G(d) geometry.

b) The quantities $|\Delta r|$, $|\Delta\theta|$, and $|\Delta\phi|$ are the absolute differences in corresponding bond lengths, bond angles, and dihedral angles, respectively, between QCISD/6-311G(d,p) and MP2/6-31+G(d) optimized geometries.

c) The dihedral angles in ethylene are all 0° or 180° by symmetry and so are not included in the comparisons.

Table II. Reactions used to validate the benchmark ΔE values. Schematic structures of the numbered species are given in Figure 1.

	Reaction	MP2/ 6-311+G(2df,2p)	MP2/ 6-31+G(d)	CCSD(T)/ 6-31+G(d)	Benchmark	Abs. Dev.[(a)]
1	$(LiCH_2Cl)_2$ **6** + Ethylene → LiCl + Cyclopropane + $LiCH_2Cl$	-18.72	-18.33	-13.18	-13.57	4.76
2	$(LiCH_2Cl)_2$ **7** + Ethylene → LiCl + Cyclopropane + $LiCH_2Cl$	-19.93	-20.19	-15.20	-14.94	5.25
3	$(LiCH_2Cl)_2$ **6** + Ethylene → TS **8** (direct)	11.00	11.23	9.57	9.34	1.88
4	$(LiCH_2Cl)_2$ **7** + Ethylene → TS **9** (direct)	8.64	7.86	5.90	6.68	1.19
5	$(LiCH_2Cl)_2$ **6** + Ethylene → TS **10** (stepwise)	21.39	24.38	26.84	23.84	0.54
6	$(LiCH_2Cl)_2$ **7** + Ethylene → TS **11** (stepwise)	15.44	17.36	19.81	17.88	0.52
7	$(LiCH_2Cl)_2$ **6** + Ethylene → PRC **10′** (stepwise)	-8.67	-8.86	-8.71	-8.52	0.34
8	$(LiCH_2Cl)_2$ **7** + Ethylene → PRC **11′** (stepwise)	-9.06	-10.40	-10.39	-9.05	1.36
					Average	1.98

[(a)] $|\Delta E_{\text{benchmark}} - \Delta E_{\text{MP2/6-31+G(d)}}|$

Table III. Mean absolute differences $\delta E = |E_{DFT//MP2} - E_{MP2}|$ and standard deviations (kcal/mol).

Functional	Gas phase (51)		THF-solvated (33)		Full test set (84)	
	Average	Std. dev.	Average	Std. dev	Average	Std. dev
PW91	0.95	1.35	2.44	1.31	1.61	1.52
mPWPW91	0.99	1.39	3.60	1.99	2.12	2.10
PBE	0.86	0.96	2.87	1.50	1.74	1.57
TPSS	0.86	1.32	3.19	1.99	1.88	2.00
M06-L	0.69	1.15	2.19	1.22	1.35	1.39
B3LYP	0.75	1.36	3.57	2.22	1.98	2.25
B3PW91	0.39	1.04	2.66	1.59	1.37	1.72
mPW1LYP	0.64	1.11	2.31	1.23	1.37	1.43
mPW1PW91	0.44	1.08	2.24	1.29	1.23	1.48
PBE0	0.33	0.42	1.79	1.11	0.96	1.07
BMK	0.63	1.00	2.50	1.21	1.26	1.40
M06	0.64	1.16	1.91	1.09	1.20	1.30
M06-2X	0.57	1.09	1.85	1.01	1.14	1.23

Table IV. Mean absolute errors in reaction energetics $\delta\Delta E_{MP2//DFT} = |\Delta E_{MP2//DFT} - \Delta E_{MP2}|$ (kcal/mol).

Model Chemistry	Gas phase			THF-solvated			Full test set		
	All	ΔE	$\Delta E^{\ddagger}$	All	ΔE	$\Delta E^{\ddagger}$	All	ΔE	$\Delta E^{\ddagger}$
Number of reactions	45	21	24	33	21	12	78	42	36
PW91	5.75	4.16	7.13	6.18	7.47	3.92	5.93	5.82	6.06
mPWPW91	5.51	5.07	5.89	6.79	9.40	2.24	6.05	7.24	4.67
PBE	5.33	3.67	6.79	6.02	7.35	3.69	5.62	5.51	5.76
TPSS	5.55	6.11	5.05	6.67	9.84	1.13	6.02	7.98	3.74
M06-L	3.21	1.91	4.36	3.21	2.72	4.06	3.21	2.31	4.26
B3LYP	4.28	6.38	2.45	7.73	10.34	3.17	5.74	8.36	2.69
B3PW91	3.20	3.82	2.65	6.44	8.47	2.90	4.57	6.15	2.74
mPW1LYP	4.11	5.88	2.56	6.74	9.00	2.78	5.22	7.44	2.64
mPW1PW91	2.86	2.86	2.87	5.47	7.24	2.38	3.97	5.05	2.70
PBE0	2.79	2.01	3.47	4.91	6.61	1.93	3.69	4.31	2.96
BMK	2.86	4.25	1.65	6.53	6.53	(a)	4.41	5.39	(a)
M06	3.12	2.34	3.80	3.23	3.31	3.11	3.17	2.82	3.57
M06-2X	2.46	2.15	2.73	2.48	2.75	2.01	2.47	2.45	2.49
MP2//PW91	0.75	0.49	0.98	2.48	2.75	2.01	0.80	0.61	1.02
MP2//mPWPW91	0.79	0.51	1.04	0.86	0.73	1.09	1.04	0.99	1.10
MP2//PBE	0.58	0.17	0.94	1.38	1.47	1.21	0.81	0.67	0.99
MP2//TPSS	0.70	0.53	0.85	1.14	1.17	1.09	0.98	0.93	1.05
MP2//M06-L	0.43	0.59	0.29	1.37	1.34	1.43	0.63	0.77	0.47
MP2//B3LYP	0.52	0.51	0.53	0.91	0.95	0.83	1.13	1.54	0.66
MP2//B3PW91	0.30	0.43	0.19	1.97	2.57	0.91	0.73	0.99	0.43
MP2//mPW1LYP	0.36	0.50	0.24	1.32	1.56	0.91	0.74	1.03	0.41
MP2//mPW1PW91	0.33	0.41	0.27	1.26	1.55	0.75	0.64	0.82	0.43
MP2//PBE0	0.18	0.08	0.27	1.07	1.24	0.77	0.54	0.56	0.50
MP2//BMK	0.37	0.64	0.13	1.14	1.14	(a)	0.70	0.89	(a)
MP2//M06	0.43	0.54	0.34	1.11	1.28	0.80	0.72	0.91	0.49
MP2//M06-2X	0.35	0.47	0.23	0.67	0.60	0.81	0.48	0.53	0.43

(a) Transition state geometries for TS **8-11** failed to converge for THF-solvated molecules with X = Cl and Br.

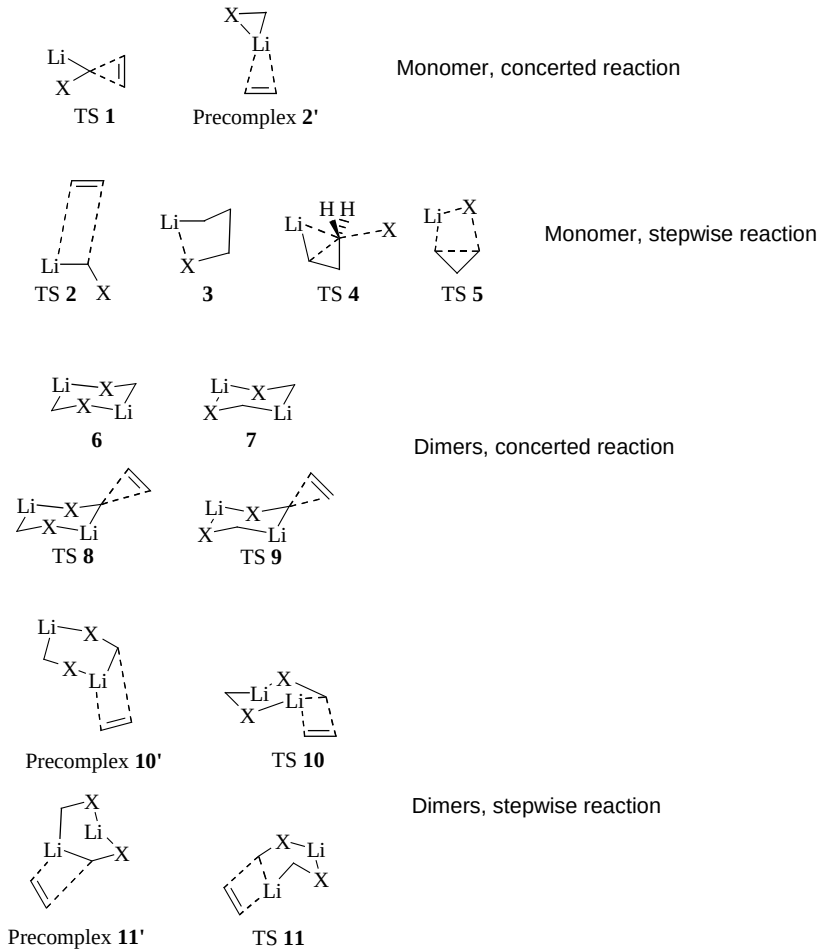

Figure 1. Structures and the numbering scheme used for the "gas phase" molecules involved in the reactions of halomethyllithiums with ethylene. Each pre-reactive complex (or pre-complex) numbered **n′** is a true minimum between the reactants and the transition state labeled TS **n**.

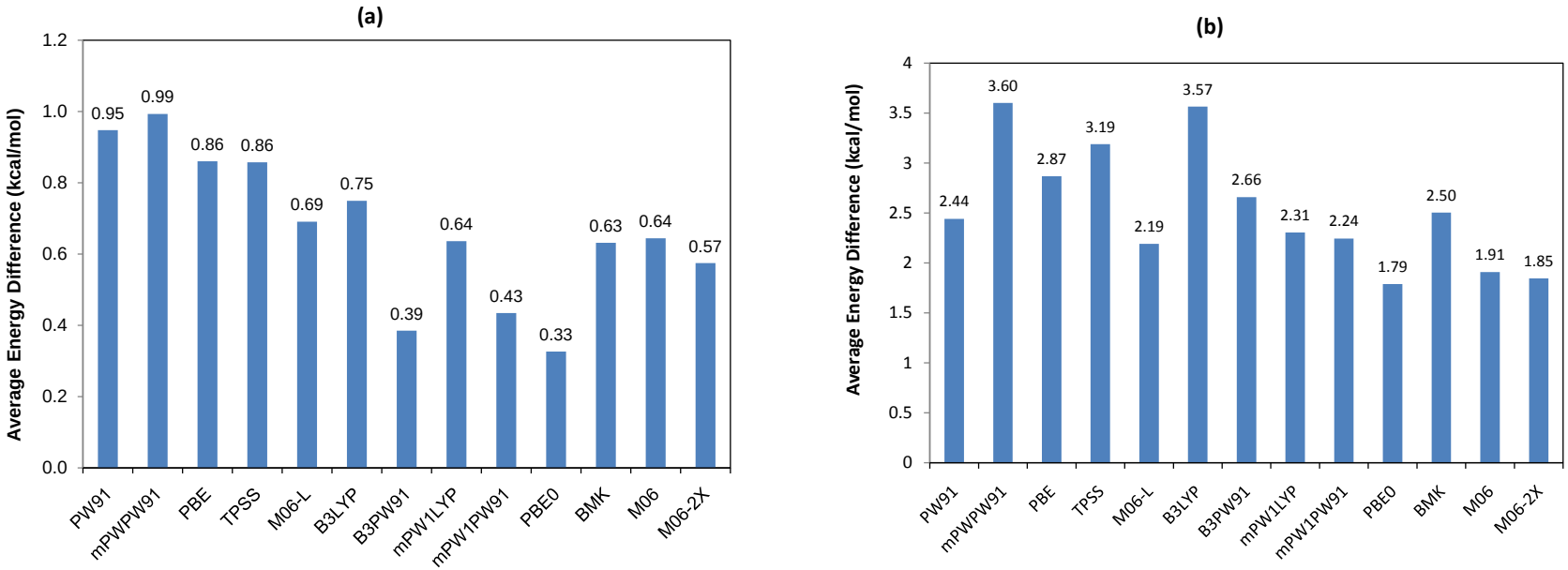

Figure 2. The average $\delta E_{DFT} = |E_{MP2//DFT} - E_{MP2}|$ for (a) the set of 51 "gas phase" molecules (i.e., none coordinated to THF, but including THF) including 24 transition state structures; (b) the set of 33 THF-solvated molecules including 12 transition states, for the 13 functionals studied.

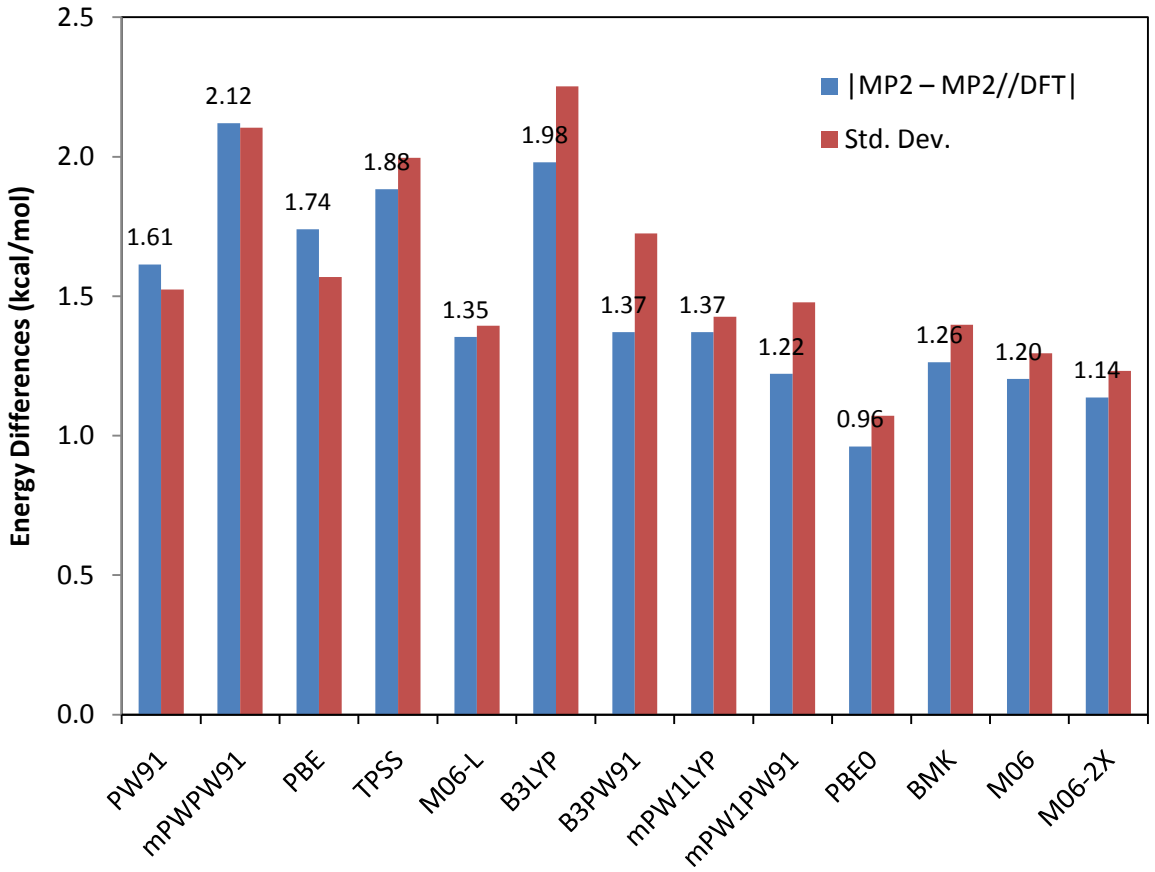

Figure 3. The average $\delta E_{DFT} = |E_{MP2//DFT} - E_{MP2}|$ for the full set of 84 molecules studied (in blue) and the standard deviation of the differences (in red). The set includes 36 transition states, 6 pre-reactive complexes with long-range non-bonded interactions, and 33 species explicitly coordinated to THF.

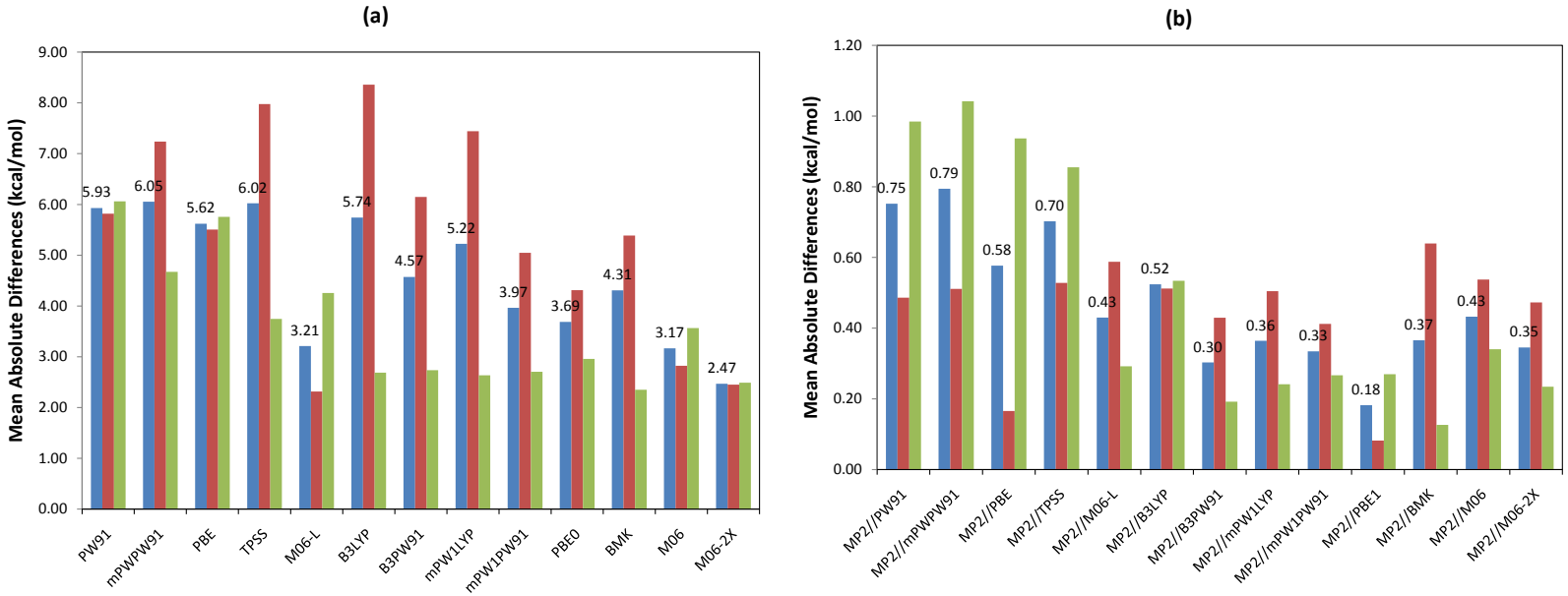

Figure 4. (a) The average $\delta\Delta E_{DFT} = |\Delta E_{DFT} - \Delta E_{MP2}|$, and (b) the average $\delta\Delta E_{MP2//DFT} = |\Delta E_{MP2//DFT} - \Delta E_{MP2}|$, for for 45 gas phase reactions considered, which include 24 reaction barriers and 9 instances in which pre-reactive complexes are formed. Blue = overall average, red = reaction energies (products – reactants) only, and green = reaction barriers (transition state – reactants) only.

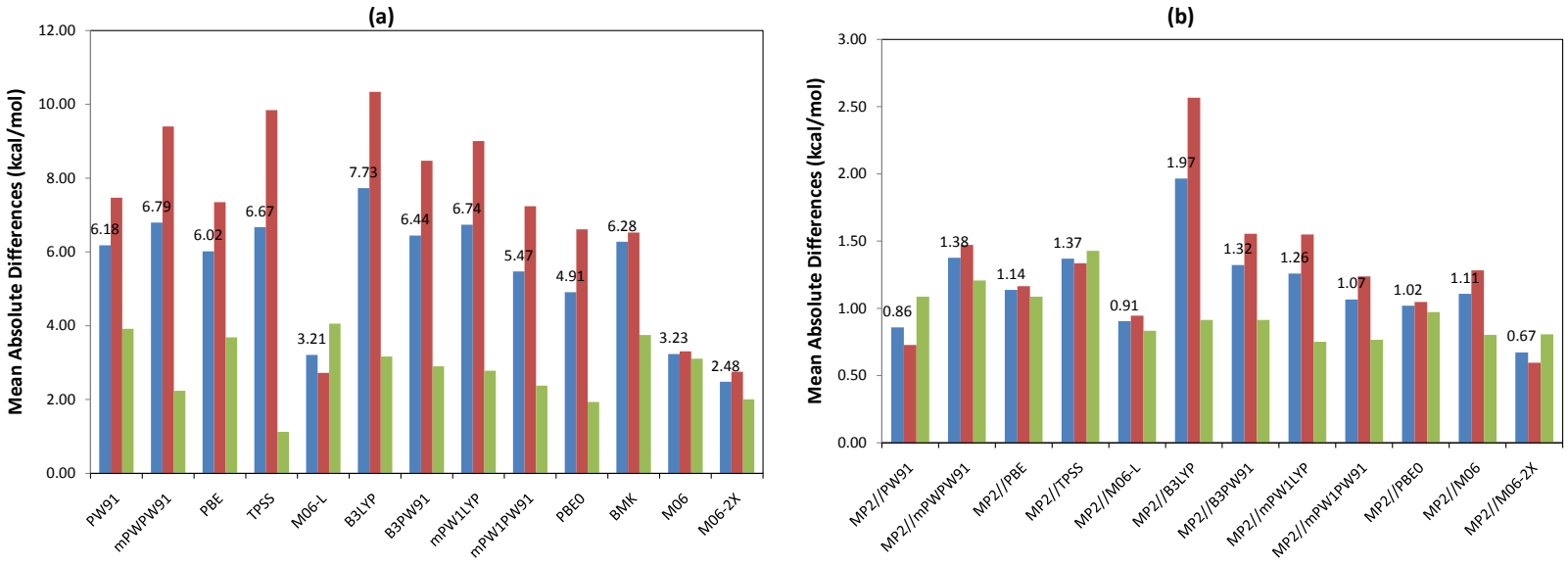

Figure 5. (a) The average $\delta\Delta E_{DFT} = |\Delta E_{DFT} - \Delta E_{MP2}|$, and (b) the $\delta\Delta E_{MP2//DFT} = |\Delta E_{MP2//DFT} - \Delta E_{MP2}|$ for for 33 reactions involving THF-solvated organolithium species, which include 12 reaction barriers. Blue = overall average, red = reaction energies (products – reactants) only, and green = reaction barriers (transition state – reactants) only.

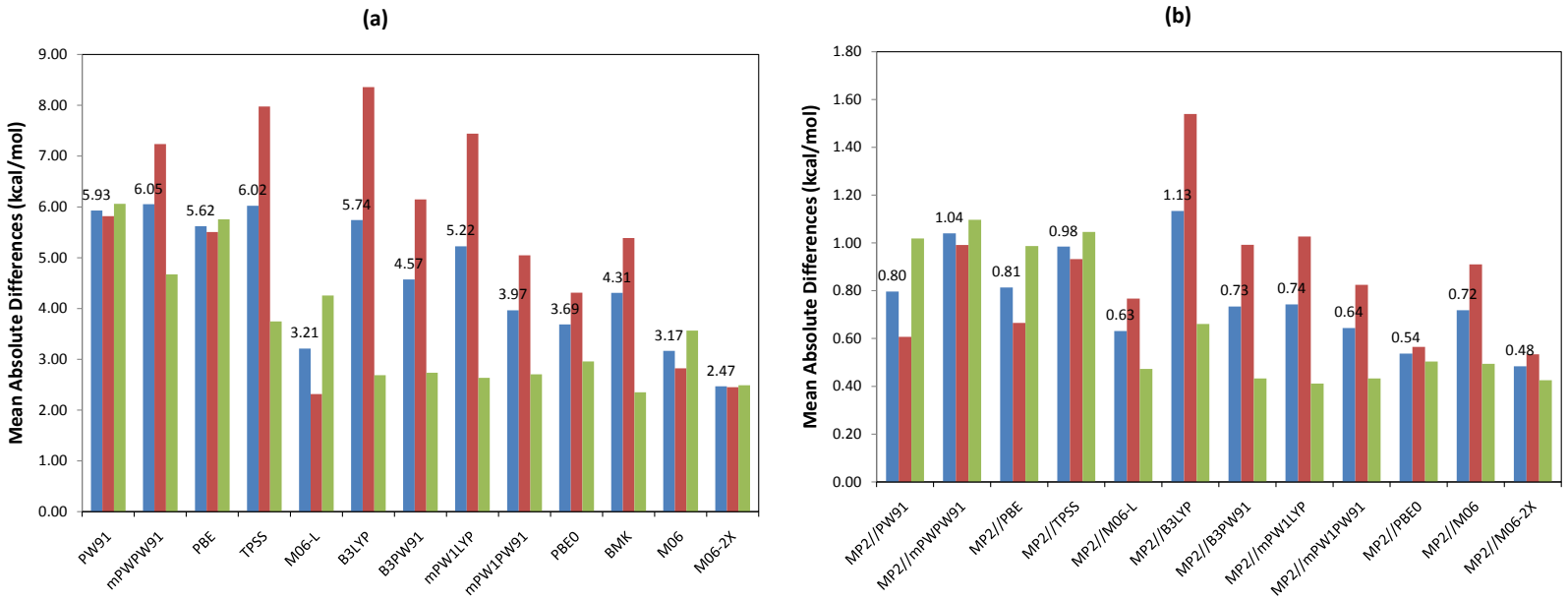

Figure 6. (a) The average $\delta\Delta E_{DFT} = |\Delta E_{DFT} - \Delta E_{MP2}|$, and (b) the $\delta\Delta E_{MP2//DFT} = |\Delta E_{MP2//DFT} - \Delta E_{MP2}|$, for full set of 78 reactions. Blue = overall average, red = reaction energies (products – reactants) only (average of 42), and green = reaction barriers (transition state – reactants) only (average of 36).

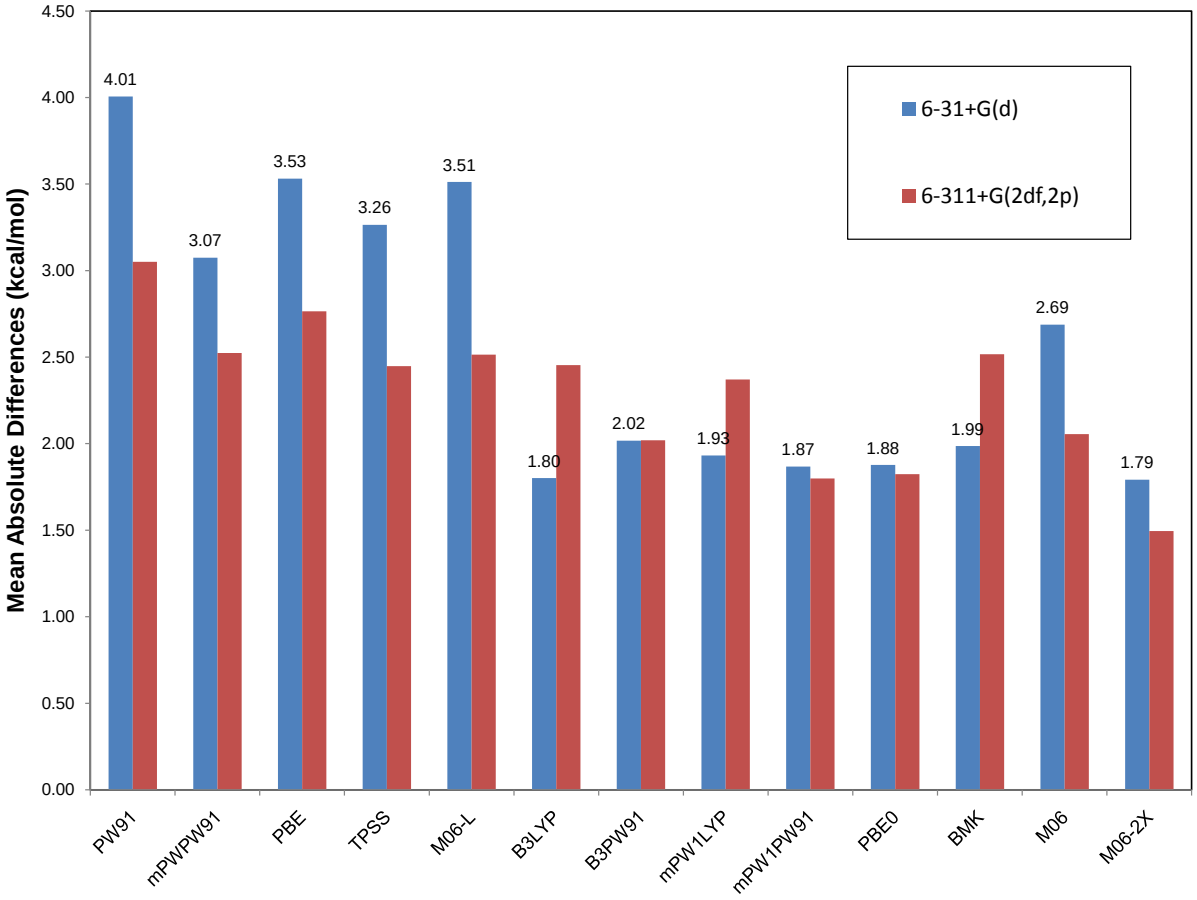

Figure 7. Mean absolute errors $\delta\Delta E_{\mathrm{DFT}}$ relative to the benchmark ΔE for the 8 reactions tabulated in Table II, as a function of basis set size. MP2/6-311+G(2df,2p) reaction energies are used for reactions 1 and 2 as explained in the text.

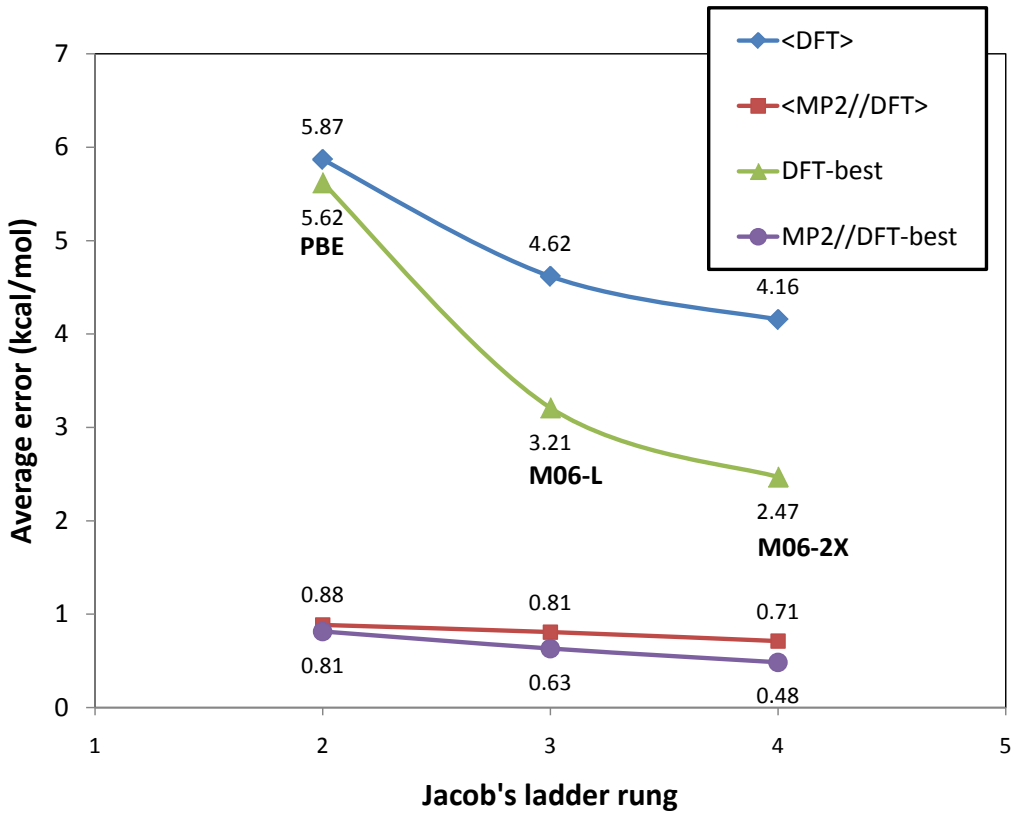

Figure 8. The average of the $\langle \delta\Delta E_{\mathrm{DFT}} \rangle$ (blue) and $\langle \delta\Delta E_{\mathrm{MP2//DFT}} \rangle$ (red) for functionals at each rung of the Jacob's ladder, and the $\langle \delta\Delta E_{\mathrm{DFT}} \rangle$ (green) and $\langle \delta\Delta E_{\mathrm{MP2//DFT}} \rangle$ (purple) for the best functionals at each rung.

Table of Contents Graphic (600 dpi TIFF; 1.37 in or 3.47 cm tall as shown below):